ACS OMEGA

http://pubs.acs.org/journal/acsodf

Article

Sawdust-Based Cellulose Nanocrystals Incorporated with ZnO Nanoparticles as Efficient Adsorption Media in the Removal of Methylene Blue Dye

Opeyemi A. Oyewo,* Amos Adeniyi, B. Bruce Sithole, and Maurice S. Onyango*

Cite This: *ACS Omega* 2020, 5, 18798−18807

Read Online

ACCESS | Metrics & More | Article Recommendations

ABSTRACT: The continuous increase in the wastes generated from forestry, timber, and paper industries has engendered the need for their transformation into economically viable materials for the benefit of mankind. This study reports the preparation and application of sawdust-derived cellulose nanocrystals (CNC) incorporated with zinc oxide as a novel adsorbent for the removal of methylene blue (MB) from water. The CNC/ZnO nanocomposite was characterized using Fourier transform infrared, X-ray diffraction (XRD), and scanning electron microscopy. The amount of MB adsorbed was determined by a UV−vis spectrophotometer. The microscopic analysis revealed that the nanocomposite had a narrow particle size range and exhibited both spherical and rod-like morphologies. The XRD analysis of the nanocomposite showed characteristic high-intensity peaks in the range of 30−75° attributed to the presence of ZnO nanoparticles, which were responsible for the enhancement of the crystallinity of the nanocomposite. The results revealed a relationship between the MB removal efficiency and changes in solution pH, nanocomposite dosage, initial concentration, temperature, and reaction time. The adsorption equilibrium isotherm, measured in the temperature range of 25−45 °C and using a concentration of 20−100 mg/L, showed that the MB sorption followed the Langmuir isotherm with a maximum adsorption capacity of 64.93 mg/g. A pseudo-second-order kinetic model gave the best fit to the experimental data. Based on adsorption performance, the CNC/ZnO nanocomposite offers prospects for further research and application in amelioration of dye-containing effluent.

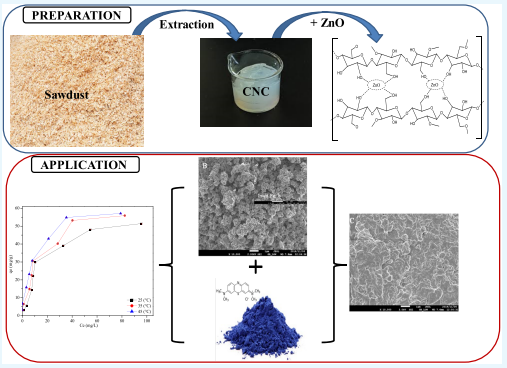

1. INTRODUCTION

Water industries face several environmental challenges, which include rapid industrialization, population growth, contamination of water sources by hazardous compounds, and the ever-increasing demands for agricultural, industrial, and domestic use.[1] As such, the release of hazardous contaminants such as pathogens, heavy metals, and dyes into the environment is now a major global concern.[2] Dyes have been reported as one of the dangerous organic pollutants that require urgent attention because they are composed of many chemicals.[3,4] The major sources of dyes in water bodies are effluents from textile, paper, rubber, plastics, paints, printing, and leather industries.[5,6] The most commonly used dye in textiles and printing industries is methylene blue (MB). It is also used as a stabilizer and an indicator in chemical industries. Consequently, effluents from these industries contain a significant amount of MB, which renders water unsuitable for both industrial reuse and domestic purposes.[7] This is because MB, even at trace levels, has significant effects on the photosynthetic activity of aquatic lives. It could also severely damage human organs by rendering the reproductive system, kidneys, central nervous system, brain, and human liver dysfunctional.[8] Therefore, the discharge of effluent-containing traces of MB dye must be treated to avoid all the dangers it poses.[9]

Removal of MB from wastewater could be achieved by different approaches, including biological, chemical, and physical methods. Some of these techniques have limitations such as low performance, non-biodegradability of MB, and generation of secondary waste that pose disposal problems. To address these challenges, photocatalysis and adsorption processes have been recognized as highly efficient methods in the removal of MB from aqueous medium.[4,10] By comparing experimental results and mathematical modeling, Shavisi et al.[11] reported insignificant differences in the performances of both adsorption and photocatalytic processes in water treatment. The simplicity in the design and operation of the adsorption technique[12] and the low energy consumption

Received: April 26, 2020
Accepted: July 3, 2020
Published: July 22, 2020

https://dx.doi.org/10.1021/acsomega.0c01924
ACS Omega 2020, 5, 18798−18807

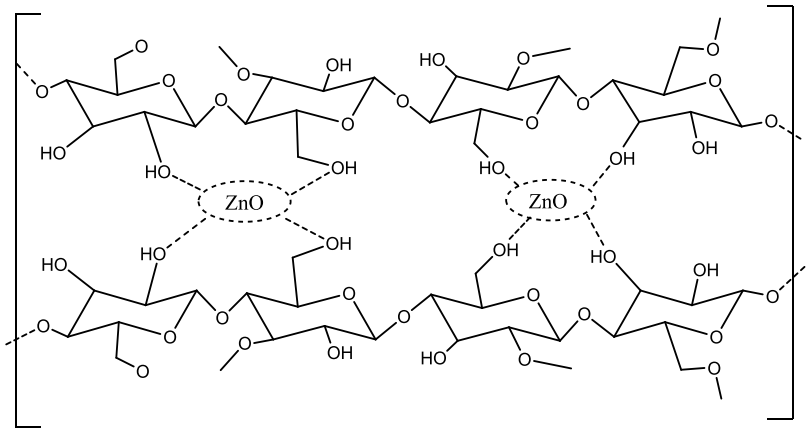

Figure 1. Proposed structure of the synthesized CNC/ZnO nanocomposite.

requirement offer high economic and practical feasibility and suitability in water pollution control, especially in dye removal from water. As a consequence, this study explores the application of adsorption in MB removal. The first step in developing an adsorption technology resides in choosing appropriate media of known kinetic and equilibrium performances.

Agro-based lignocellulosic biomasses are gaining more attention in the adsorption process because they embody some useful components necessary in water treatment.[13] They are eco-friendly and abundantly available.[14,15] In a critical review by Charis et al.,[16] it was found that waste generated from sawmills in Zimbabwe and South Africa amounted to about 70,000 tons per annum. Sawdust and shavings represent the most underutilized waste fractions, with heaps scattered all over the region and posing various ecological threats. By using a comparative cost−benefit analysis and the reported feasibility studies, utilization of sawdust via transformation is highly recommended.[17,18] In our previous studies, cellulose nanocrystals (CNC) extracted from this waste have been proven to be highly efficient in water treatment.[19,20] However, the limitation of low density, which resulted in an unstable adsorbent powder material, cannot be overlooked. Thus, this challenge could be addressed by the introduction of eco-friendly nanoparticles as a filler to improve the density and stability of the cellulose nanocrystals. The material of choice in this regard is zinc oxide.

Zinc oxide (ZnO) is a representative of a class of metal oxide that has received considerable attention owing to many of its attractive features such as environmental friendliness, high adsorption capacity, non-toxicity, and cost-effective production.[21] These properties favor its potential utility in environmental and biological applications. At the nanoscale level, ZnO exhibits interesting electronic, optoelectronic, and adsorptive properties. Studies on the adsorptive affinity of ZnO on various pollutants have been widely reported.[22] ZnO nanoparticles possess high surface area and good chemical stability, and a band gap energy of 3.37 eV allows them to absorb light in the UV region.[23,24] Therefore, the good biodegradability and biocompatibility of zinc oxide in conjunction with the good mechanical properties of cellulose nanocrystals derived from sawdust could be beneficial in the development of green nanocomposites that could be very useful in wastewater remediation. ZnO has been successfully incorporated into cellulosic materials in different reports using either tedious synthesis procedure or commercially procured cellulose in addition to some other toxic chemical additives being utilized.[25−29] This could obviously alter the quality of the material and render it environmentally unfriendly.

This study explores the conversion of sawdust-derived CNC into high-value chain green nanocomposites by the incorporation of ZnO nanoparticles, which possess a very good photocatalytic property. Some physicochemical properties of the nanocomposite were investigated to relate them to the performance achieved. Batch adsorption experiments were performed, and the nanocomposite dosage, solution pH, contact time, initial MB concentration, and temperature were varied to obtain the maximum adsorption conditions for the MB dye. More so, the CNC and ZnO were utilized separately to establish their capacities and contribution to MB removal.

2. MATERIALS AND METHODS

2.1. Materials. Deionized water from a Purite water system (model Select Analyst HP40, United Kingdom) was used for the preparation of 1 g/L MB stock solution and the nanocomposite. Cellulose nanocrystals (CNC) were supplied by CSIR-Durban, South Africa. Other chemicals including zinc oxide nanoparticles, methylene blue, NaOH, and HCl were obtained from Sigma-Aldrich, South Africa and were of analytical grade. The pH was adjusted using 0.1 M NaOH or 0.1 M HCl.

2.2. Methods. *2.2.1. Synthesis of the CNC/ZnO Nanocomposite.* The extraction of CNC from sawdust has been reported elsewhere.[30] Briefly, the procedure involved a one-pot synthesis route using deionized water and sulfuric acid, which were subsequently ultrasonicated to produce a cellulose nanocrystal suspension. The cellulose nanocrystal suspension and ZnO powder (2:1) were stirred in 1 M NaOH solutions separately for 30 min. ZnO solution was then ultrasonicated for another 2 h to ensure complete homogeneity. Afterward, the ZnO solution was added dropwise to the cellulose nanocrystals derived from the sawdust solution, and the mixture was allowed to stir for 24 h. The product, hereafter referred to as nanocomposite, was centrifuged and washed twice to remove excess materials until the pH was neutral. The centrifuged nanocomposite was then air-dried at room temperature for 3 days. At the end of the drying period, the nanocomposite was crushed and kept for use in adsorption and characterization experiments. The material was double washed after the preparation until the pH was slightly above neutral

https://dx.doi.org/10.1021/acsomega.0c01924
ACS Omega 2020, 5, 18798−18807

(7.50) before use.[31] The proposed structure of the synthesized CNC/ZnO nanocomposite is presented in Figure 1.

2.2.2. Characterization of the Synthesized CNC/Zn Nanocomposite. The raw and spent CNC/ZnO nanocomposites were characterized and compared with the pristine CNC reported in our previous study.[19] The characterization of the materials was carried out using a (i) Perkin Elmer Spectrum 100 FT-IR spectrometer, recorded in the 500−4000 cm^{-1} range at a resolution of 4 cm^{-1}; (ii) a JEOL JSM-7600F field emission scanning emission microscope (FESEM) coupled with an EDX analyzer, running at 2 kV accelerating voltage, for the morphology and elemental composition of the materials; and (iii) an X-ray diffractometer (PANalytical Empyrean) running at a voltage of 45 kV and current of 40 mA and with a monochromatic Cu Kα radiation (λ = 0.15406 nm) over a scan range of 5.0149−89.9809° for the determination of crystallinity. The phase identification analyses were further investigated using a high score plus program. The peaks obtained from the experiment were compared with the X-ray diffraction (XRD) peaks in the program database.

2.2.3. Adsorption Experiment. Factors affecting the adsorption process, which include the initial concentration of the MB dye, solution pH, CNC/ZnO dosage, and temperature, were examined in a batch system. Initially, the effect of solution pH was explored between pH 2 and 10 by adjusting a 100 mg/L solution of MB using either NaOH (0.1 M) or HCl (0.1 M). Thereafter, 0.1 g of the CNC/ZnO nanocomposite was added to the prepared solution separately in 100 mL plastic bottles to determine the optimum pH for the process. The bottles were placed in a thermostatic bath shaker running at a speed of 200 rpm for 24 h. The samples were then filtered using Whatman filter paper no. 42, and the filtrates were analyzed by UV−vis spectroscopy to determine the residual concentration of MB. The above procedure was repeated to determine the effect of CNC/ZnO dosage, initial concentration, and temperature on the amount of MB adsorbed. The effect of the initial concentration of MB was investigated between 5 and 100 mg/L, and the CNC/ZnO dosage was explored by varying the mass from 0.01 to 0.3 g. The percentage removal of MB (efficiency), R_t, was calculated using eq 1, while the amount of MB adsorbed at equilibrium, q_e, was calculated using eq 2:

$$R_t = \frac{C_o - C_e}{C_o} \cdot 100 \quad (1)$$

$$q_e = \frac{C_o - C_e}{m} \cdot V \quad (2)$$

where C_o and C_e are the initial and equilibrium concentrations (mg/L) of MB, respectively, q_e is the adsorption capacity at equilibrium (mg/g), v is the volume (L) of solution, and m is the mass (g) of the nanocomposite.

Meanwhile, sorption kinetic experiments were conducted using a batch reactor operated at a stirring speed of 300 rpm and a temperature of 25 °C. In the kinetic experiments, 2 g of the CNC/Zn nanocomposite was added to the reactor containing 1 L of MB synthetic wastewater. Effects of the initial concentration of MB were explored between 50 and 150 mg/L. At 5 min time interval, 10 mL of aliquots was withdrawn from the reaction using a syringe. Each sample was immediately filtered using a Whatman filter paper no. 42, and the filtrates were analyzed by UV−vis spectroscopy at a wavelength of 605.1 nm. The amount of MB removed at any given time was calculated using the expression below:

$$q_t = \frac{C_o - C_t}{m} V \quad (3)$$

where q_t is the time-dependent amount of MB adsorbed per unit mass of adsorbent and C_t is the concentration of MB at any time t. All the adsorption experiments were conducted in triplicate, and the average values are reported. Desorption of MB from the surface of the spent adsorbent was also investigated using three different eluents including deionized water, NaCl, and HCl. The dried spent CNC/ZnO was dispersed in these eluents separately, and the mixtures were placed in a thermostatic bath shaker operated at 160 rpm and at 25 °C for 24 h. Thereafter, the desorbed solution was analyzed and the cyclic adsorption−desorption was performed four times to establish the reusability of the adsorbent.

3. RESULTS AND DISCUSSION

3.1. Sample Characterization. *3.1.1. X-ray Diffraction (XRD) Analysis.* X-ray diffraction analyses of pristine CNC, raw CNC/ZnO nanocomposite, and spent CNC/ZnO nanocomposite displayed peaks associated with crystalline cellulose at 2θ = 15 and 22.5° ($C_{60}H_{88}O_8$ and $C_2H_{192}N_{64}O_{16}$), which were assigned to the 1α and 1β phases of cellulose,[32] respectively, as presented in Figure 2. Upon the incorporation

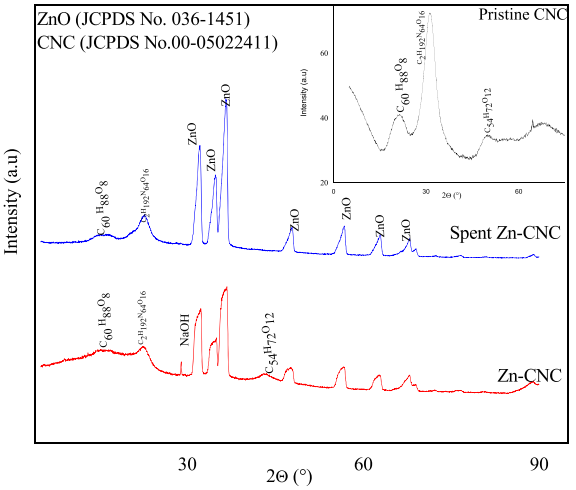

Figure 2. X-ray diffraction patterns of pristine CNC, raw CNC/ZnO nanocomposite, and spent CNC/ZnO nanocomposite.

of ZnO into cellulose, some broad peaks appeared at 2θ = 30.1, 35.2, 48.3, and 72°, which are the (100), (002), (102), and (201) lattice planes of hexagonal wurtzite ZnO, respectively.[33] The standard JCPDS pattern for ZnO used is 036-1451, while for the extracted cellulose nanocrystals, the JCPDS number is 00-050-22411. This confirmed the nanocomposite formation. Also, a narrow peak appeared around 2θ = 25.1°, indicating the presence of sodium hydroxide, which was used as a solvent in the synthesis of the nanocomposite. The disappearance of peaks associated with $C_{54}H_{72}O_{12}$ from the diffraction pattern of the spent CNC/ZnO nanocomposite occurred, suggesting the involvement of this phase in the process of MB adsorption onto the nanocomposite.[34]

3.1.2. Fourier Transforms Infrared (FT-IR) Spectroscopy. FT-IR analyses were carried out to identify the associated functional groups of pristine CNC, raw CNC/ZnO nanocomposite, and spent CNC/ZnO nanocomposite. The spectra were recorded in the range of 400−4000 cm^{-1} and are

https://dx.doi.org/10.1021/acsomega.0c01924
ACS Omega 2020, 5, 18798−18807

presented in Figure 3. The spectra of the raw and spent CNC/ZnO nanocomposite showed a peak between 3286 and 3486

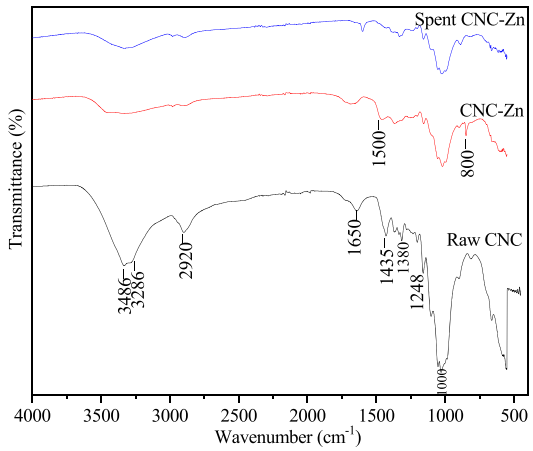

Figure 3. FT-IR spectra of pristine CNC, raw CNC/ZnO nanocomposite, and spent CNC/ZnO nanocomposite.

cm^{-1} attributed to the O−H stretching vibration. The intensity of this vibration was reduced after incorporating ZnO into cellulose, which indicated the involvement of the oxygen atom in the bonding interaction with ZnO resulting in the weakening of the O−H bond strength. The intermolecular hydrogen bonds in pristine CNC enhance its reactivity when participating in a chemical reaction. A band peak around 1000 cm^{-1} was ascribed to the stretching vibration of C−O, while the peak at 1435 cm^{-1} is attributed to the CH_2 vibration and it is regarded as a crystallinity band in any cellulosic material; the frequency of vibration of this peak becomes smaller in the spent adsorbent, suggesting the entrapment of MB onto the surface. The absorption peak around 2920 cm^{-1}, which corresponds to the C−H vibration of sp^3-hybridized carbon, disappeared upon nanocomposite formation and after adsorption.[19] The intensity of this peak was found to decrease with ZnO loading, which could be an indication for the presence of ZnO within the lattice of CNC. A similar observation has been reported in a study involving cellulose-based nanocomposites.[32,33]

3.1.3. Scanning Electron Microscopy Analysis. The details of the morphological properties of pristine CNC have been extensively reported in our previous study.[19] The material exhibited particles of similar length and width, however not very dense. An increase in the density of the material could be observed upon the formation of the nanocomposite, which was due to the presence of zinc oxide nanoparticles as shown in Figure 4A,B. The micrograph of the raw CNC/ZnO nanocomposite displayed a spherical shape with a rough surface Figure 4B. The fibers appeared to be swelled up with an increase in diameter, which is obviously due to the presence of ZnO nanoparticles on the surface of the material. Furthermore, the micrographs of the raw and spent CNC/ZnO nanocomposite confirmed the incorporation of ZnO nanocrystals on the CNC matrices (Figure 4B,C). This could be inferred from the agglomeration observed in the micrograph upon nanocomposite formation and after the adsorption process. The observed agglomeration could be as a result of the weak forces between the particles.[35] An increase in agglomeration could also be noticed in the SEM micrograph of the spent nanocomposite, and this might be due to the increase in the moisture content as a result of dye molecules attached. A similar observation has been reported in nanocomposite formation involving ZnO.[36,37]

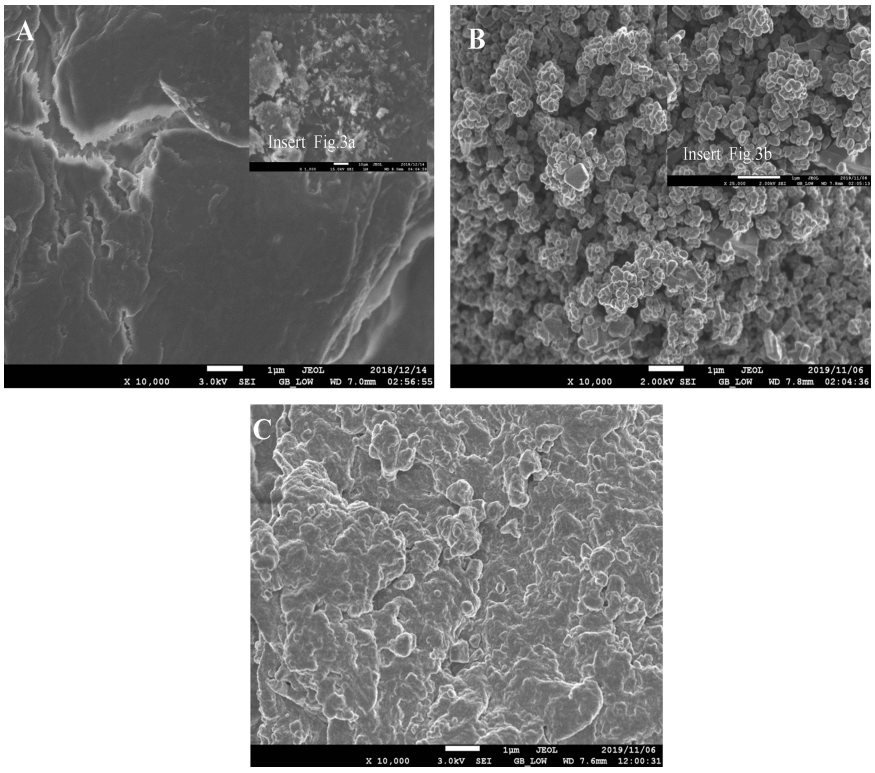

Figure 4. SEM images of (A) pristine CNC, (B) raw CNC/ZnO nanocomposite, and (C) spent CNC/ZnO nanocomposite.

https://dx.doi.org/10.1021/acsomega.0c01924
ACS Omega 2020, 5, 18798−18807

3.2. Adsorption Studies. *3.2.1. Effect of Dye Solution pH.* Solution pH is a very important factor that affects the ionic species of both the adsorbate and adsorbent. The effect of the solution pH was investigated in the range of pH 2 to 10, as summarized in Figure 5. MB usually exists in two forms: one

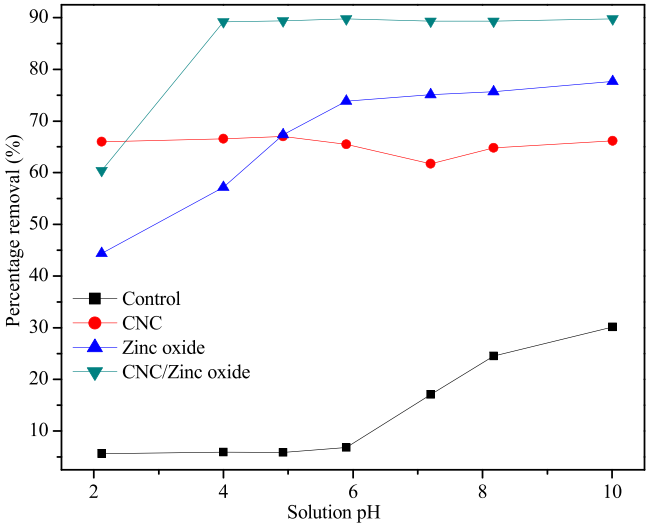

Figure 5. Effects of solution pH on MB removal from aqueous solution (dosage: 0.1 g, initial conc.: 100 mg/L, volume: 50 mL, and temp.: 25 °C)

characterized with positive charges, which is predominant in acidic medium, and the zwitterion species, which exists in alkaline conditions.[38] The experimental data obtained from the pH control studies on the MB solution displayed little or no removal of dye from pH 2 to 6. However, a slight increase in the removal capacity was noticed in the alkaline region, and this might be due to the presence of MB zwitterion species, which usually exist in this range. A similar trend of increased removal capacities with an increase in pH was observed when both CNC and zinc oxide were used in their natural forms. CNC can bind dye molecules strongly through the interaction of the hydrogen bonding, the $\pi-\pi$ interaction, and the electrostatic interaction between the positive charge of the dye and the negatively charged site of CNC.[39] The ZnO performance might be related to its photocatalytic potency as a semiconductor, which absorbs light in the UV region of the solar spectrum.[40,41] Furthermore, the incorporation of zinc oxide to the surface of CNC displayed improved performance in the removal of the MB dye from pH 4.0 with a percentage removal of 90%. At a low pH, the MB dye could enter into the pores of the CNC/ZnO nanocomposite structure and become less stable, which tends to enhance the removal efficiency of MB.[38] The formation of zwitterions species from MB solution in water is also likely responsible for the higher removal in the alkaline region.[23,24]

3.2.2. Effect of CNC/ZnO Nanocomposite Dosage. The effect of adsorbent dosage on the removal of MB is shown in Figure 6. The CNC/ZnO dosage was varied from 0.01 to 0.30 g. The results show an increase in the adsorption efficiency of the CNC/ZnO nanocomposite with an increase in dosage. This is obviously due to an increase in the adsorbent's active sites. A maximum adsorption percentage removal of 97.5% was achieved with 0.15 g of the nanocomposite.

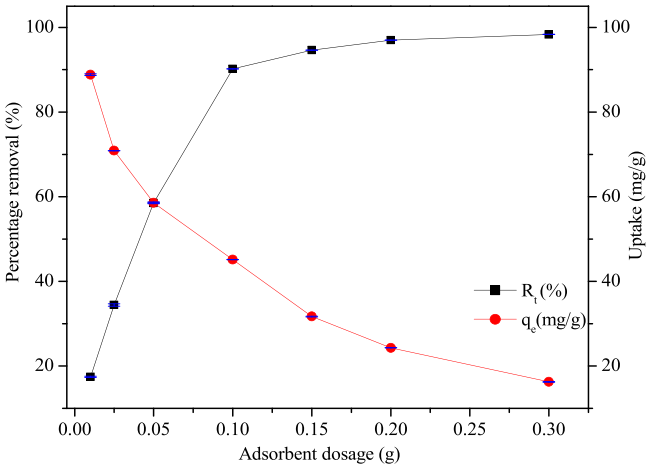

Figure 6. Effects of CNC/ZnO nanocomposite dosage on MB removal from aqueous solution (initial conc.: 100 mg/L, volume: 50 mL, and temp: 25 °C).

3.3. Adsorption Isotherms. The concept of the adsorption process is usually described by the adsorption isotherm. Temperature ranges from 25 to 45 °C were explored to determine the relationship between the equilibrium concentration (C_e) of the adsorbate (dye) and the adsorption capacity (q_e) of the adsorbent (CNC/Zn nanocomposite) (Figure 7).[42] As such, a direct relationship is observed between

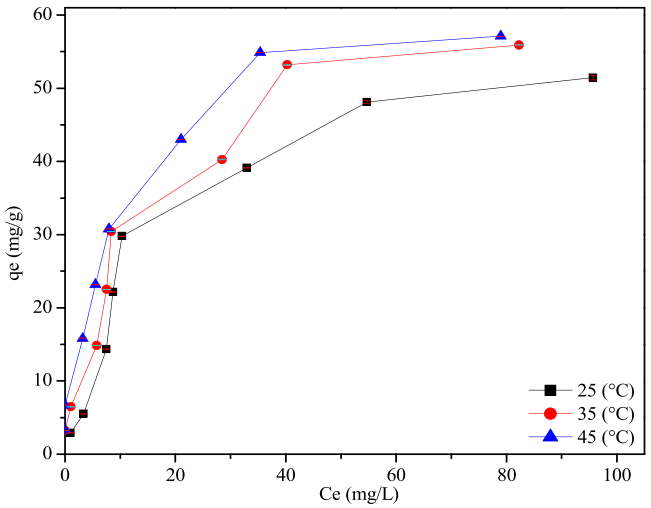

Figure 7. Adsorption equilibrium isotherms of MB onto the modified CNC/ZnO nanocomposite.

the temperature and the MB removal efficiency, and this might be due to the temperature-induced increase in the rate of diffusion of MB across the external boundary layer and into the internal pores of the nanocomposite. The data obtained from sorption equilibrium were then used to describe the interaction between adsorbate and the adsorbent. For this purpose, two common adsorption equilibrium models including Langmuir and Freundlich isotherm models were adopted.

The Langmuir isotherm model assumes that the adsorption occurs at specific binding sites localized on the homogeneous surface of the adsorbent, which could only be covered by single or monolayer. Thus, all adsorption sites are considered equivalent and identical. On the other hand, the Freundlich adsorption model is used to explain the multilayer adsorption

https://dx.doi.org/10.1021/acsomega.0c01924
ACS Omega 2020, 5, 18798−18807

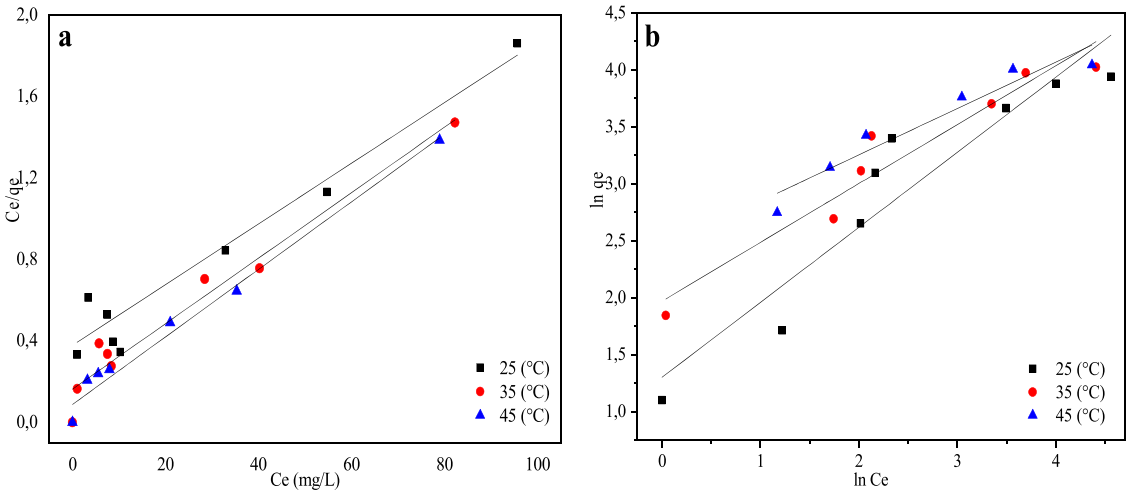

Figure 8. Fitting of adsorption isotherm models: (a) Langmuir isotherm model. (b) Freundlich isotherm model.

on the surface of adsorbent in a non-uniform manner.[43] The linear form of the Langmuir and Freundlich equations is presented in eqs 4 and 5, respectively:

$$\frac{C_e}{q_e} = \frac{C_e}{q_m} + \frac{1}{k_L q_m} \quad (4)$$

$$\ln q_e = \ln k_F + \frac{1}{n} \ln C_e \quad (5)$$

where C_e is the equilibrium concentration of the MB dye (mg/L), q_e is the amount of MB adsorbed on the adsorbent at the equilibrium (mg/g), q_m is the maximum adsorption capacity, which describes a complete monolayer adsorption (mg/g), k_L is a Langmuir isotherm constant (L/mg) related to the free energy of adsorption, and k_F and n are the Freundlich constants.

Figure 8a,b displays the linearized Langmuir and Freundlich plots, respectively, for the adsorption of methylene blue onto the CNC/ZnO nanocomposite. From these plots, the isotherm parameters were obtained and are summarized in Table 1. It is

Table 1. Summary of Equilibrium Isotherms Parameters of MB Sorption onto the CNC/ZnO Nanocomposite

	Langmuir isotherm parameters			Freundlich isotherm parameters		
temperature (°C)	q_m (mg/g)	b (L/mg)	R^2	k_F (L/g)	$1/n$	R^2
25	60.24	5.283	0.998	3.67	0.66	0.8968
35	62.10	6.016	0.999	5.336	0.61	0.9176
45	64.93	22.39	0.999	6.203	0.60	0.8887

observed that, as the temperature is increased, the Langmuir isotherm parameters also increase. For instance, the Langmuir maximum adsorption capacity (q_m) increased from 60.24 to 64.93 mg/g with an increase in temperature from 25 to 45 °C. Similarly, the Freundlich isotherm parameters k_F and $1/n$ displayed the same trend as the temperature increased. From the values of the correlation coefficients, the adsorption of MB onto the CNC/ZnO nanocomposite is well described by the Langmuir adsorption isotherm in the investigated temperature range. Meanwhile, a comparison of the Langmuir capacity of the CNC/ZnO nanocomposite with other biomaterials shows that the capacity obtained in this study is quite competitive (see Table 2).

Table 2. Comparison of Uptake Values between the CNC/ZnO Nanocomposite and Different Adsorbents in Methylene Blue Removal

adsorbent product	MB treated	time (min)	temp. (°C)	q_m (mg/g)	references
CNC/ZnO nanocomposite	MB	1440	45	64.93*	this study
β-cyclodextrin−chitosan nanoparticles	MB	50	30	2.78	44
Celite-sodium alginate bio-polymer	MB	120	60	7.5	45
λ-carrageenan-calcium phosphate-sodium alginate biopolymer	MB	120	60	6.8	45
carboxyl methylcellulose-sodium alginate biopolymer	MB	120	60	6.5	45
Moroccan cactus (Natural (NC))	MB	60	25	3.44	46
dried cactus (DC)	MB	60	25	14.04	46
sago waste (*Metroxylon* spp.)	MB	2880	25	36.6	47
sugar scum	MB	600	25	24.52	48

3.4. Adsorption Kinetics. The competitive uptake capacity of the CNC/ZnO nanocomposite obtained in the equilibrium determination experiment prompted us to further study the adsorption kinetic process. The experiments were conducted using an initial concentration of MB in the range of 50−150 mg/L and using 2 g of CNC-nanocomposite in a liter of MB solution. As shown in Figure 9, fast adsorption is observed at the initial stage due to the availability of an ample number of active sites, which then slowed down after 25 min in the MB concentration range investigated. The time required for the adsorption of MB to reach equilibrium using the CNC/ZnO nanocomposite was found to be less than 2 h. This indicates that the rate of the diffusion of adsorbate into the CNC/ZnO nanocomposite pores is very rapid.[49] To further investigate the adsorption phenomenon, kinetic models, pseudo-first-order (eq 6) and pseudo-second-order (eq 7) models, were employed and the obtained parameters are summarized in Table 3:

https://dx.doi.org/10.1021/acsomega.0c01924
ACS Omega 2020, 5, 18798−18807

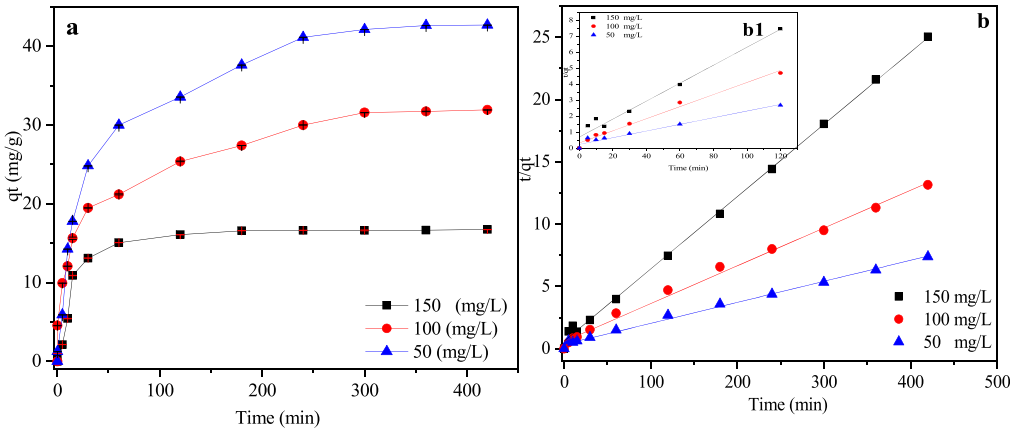

Figure 9. (a) Adsorption kinetics for MB onto the CNC/ZnO nanocomposite at different concentrations (dosage: 2 g, volume: 50 mL). (b) Pseudo-second-order model and (b1) pseudo-second order model for early-stage kinetic data.

Table 3. Kinetic Parameters for MB onto the CNC/ZnO Nanocomposite

	pseudo-first-order model parameter			pseudo-second-order model parameter		
C_o (mg/L)	a (g/mg·min)	$b \times 10^{-3}$ (mg/g)	R^2	q_e (mg/g)	$k_2 \times 10^{-3}$ (g/mg·min)	R^2
50	1.03	1.26	0.912	17.153	0.007	0.999
100	2.95	1.78	0.921	32.68	0.002	0.999
150	10.08	1.95	0.943	59.17	0.001	0.994

$$\log(q_e - q_t) = \log q_e - \frac{k_1}{2.303}t \quad (6)$$

$$\frac{t}{q_t} = \frac{1}{k_2 q_e} + \frac{1}{q_e}t \quad (7)$$

where q_e and q_t are the adsorption capacity (mg/g) of the solute at equilibrium and at time t (min), respectively, k_1 (min^{-1}) and k_2 (g/mg·min) are the rate constants of the pseudo-first-order and pseudo-second-order adsorption, respectively.

From Table 3, it is seen that the pseudo-second-order model describes the kinetics of MB adsorption onto the CNC/ZnO nanocomposite. The linear regression values obtained using this model gave a higher correlation coefficient (R^2) of >0.99 compared to the pseudo-first-order model.

The fit to pseudo-second-order is also illustrated in Figure 9b wherein linear curves are observed further, confirming the applicability of the model to describe the adsorption process. The fact that the adsorption process follows the pseudo-second-order model may suggest that the MB interaction with adsorption sites was chemical in nature. Given the nature of the scale used in the linearized form of the pseudo-second-order model, it was suggested that chemical adsorption contributed to maximum MB adsorption from simulated water. To confirm this, the early stage of kinetic experimental data was also modeled with pseudo-second-order kinetics (Figure 9b1). In light of this evidence, adsorption kinetics of MB onto the CNC/ZnO nanocomposite is mainly diffusion-based mechanisms whereby different adsorption sites on a homogeneous solid substrate randomly collide with each other and diffuses through the adsorbent pore size during a rate-limiting mechanistic step.[50]

3.5. Thermodynamic Study. Thermodynamic study provides further information about the adsorption mechanism of CNC/ZnO on MB; therefore, temperature ranges of 298–338 K were investigated. All the thermodynamic parameters such as enthalpy (ΔH), entropy change (ΔS), and the standard Gibbs free energy (ΔG) were calculated from the van't Hoff equation demonstrated the dependence of equilibrium constant on temperature as follows:

$$\ln K_d = -\frac{\Delta H}{RT} + \frac{\Delta S}{R} \quad (8)$$

$$\Delta G = -RTK_d \quad (9)$$

where T (K) is the temperature in Kelvin and R (8.314 J/mol·K) is the universal gas constant.

Thermodynamic parameters presented in Table 4 shows the positive value of enthalpy $\Delta H°$, which confirmed that the adsorption of MB onto CNC/ZnO was endothermic in nature, while the positive value of $\Delta S°$ indicated that the randomness at the solid/solution interface increased. This was due to the fact that the water molecules that were displaced by the adsorbate species gained more transitional energy than was lost by the adsorbate ions.[51] The negative values of $\Delta G°$ indicated that the adsorption mechanism of MB onto the CNC/ZnO nanocomposite was a favorable spontaneous process. According to some studies,[52,53] a value of enthalpy $\Delta H° < 84$ kJ/mol represents physisorption while the values between 84 and 420 kJ/mol are considered to be chemisorption. Therefore, it is an indication that the interaction mechanism for the sorption of MB onto CNC/ZnO could be chemical interaction.

Table 4. Thermodynamic Parameters for MB Sorption onto CNC/ZnO

temp (°C)	$\Delta G°$ (kJ/mol)	$\Delta H°$ (kJ/mol)	$\Delta S°$ (kJ/mol·K)
25	−263.9	166.9	48.86
35	330.6		
45	393.7		

3.6. Adsorption–Desorption Studies. The adsorption–desorption experiments were investigated to establish the

https://dx.doi.org/10.1021/acsomega.0c01924
ACS Omega 2020, 5, 18798–18807

adsorbent economic viability and also to eradicate the secondary pollution that might occur via the disposal of spent CNC/ZnO composites. Three different eluents were utilized for desorption preliminary studies; however, the 2.5 M sodium chloride solution was found to be more efficient. Therefore, this concentration was chosen for the subsequent desorption process. The adsorption−desorption procedure was repeated four times, and the percentage desorption efficiency for each cycle was determined using eq 10 as follows:

$$\%\text{desorption efficiency} = \frac{\text{released MB concentration}}{\text{initial adsorbed MB}} \quad (10)$$

The adsorption−desorption results are presented in Figure 10. From the graph, a decrease in the adsorption and

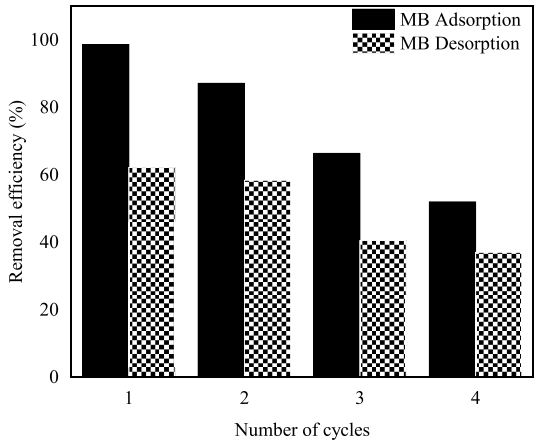

Figure 10. Adsorption−desorption efficiency of MB using 2.5 M NaCl eluents.

desorption efficiencies could be noticed in each operation cycle. In each cycle, the adsorption efficiency was higher than that of desorption, thereby indicating that the recovered CNC/ZnO still possessed a high adsorption capacity even after four cycles of desorption−adsorption.

Consequently, only 50% reduction in adsorption percentage was observed after the fourth cycle. This thus confirmed that not all active sites were released during the desorption step, causing the adsorbent to lose its activity. The decrease in desorption efficiency in each cycle was a manifestation of the strong bonds formed between the adsorbing MB and active sites. In addition, the subsequent loss in adsorbent mass and the dissolution of CNC/ZnO could also affect the adsorption mechanisms between MB and the composite.[54] Overall, the competitive result obtained in this study is an indication that the CNC/ZnO nanocomposite could be reused efficiently with less loss of capacity. Similar observations were reported in the adsorption−desorption of reactive dyes.[55]

4. CONCLUSIONS

In this study, the sawdust-derived CNC/ZnO nanocomposite was successfully synthesized, characterized and utilized for the adsorption of MB from simulated water. Physicochemical properties of the raw CNC, CNC/ZnO nanocomposite, and spent CNC/ZnO nanocomposite were analyzed using the appropriate analytical techniques. Indeed, the CNC/ZnO nanocomposite exhibited high removal of MB compared to raw CNC and ZnO in their natural form. The adsorption of MB onto CNC/ZnO occurred at specific homogeneous binding sites, which could only be covered by single or monolayer, thus conformed to the Langmuir isotherm model. Fast adsorption at the initial stage was also observed from kinetic results, which are attributed to the availability of an ample number of active sites. The kinetic experimental data conformed to the pseudo-second-order model, with a high correlation coefficient of 0.999 in all cases. Overall, the CNC/ZnO nanocomposite has been proven as an efficient and eco-friendly adsorbent, which could be useful in the remediation of water from dye pollution.

AUTHOR INFORMATION

Corresponding Authors

Opeyemi A. Oyewo − *Department of Chemical, Metallurgical and Materials Engineering, Tshwane University of Technology, Pretoria 0001, South Africa;* orcid.org/0000-0002-7229-8104; Phone: +27123823596; Email: Atiba.opeyemi@gmail.com

Maurice S. Onyango − *Department of Chemical, Metallurgical and Materials Engineering, Tshwane University of Technology, Pretoria 0001, South Africa*; Phone: 0123823533; Email: OnyangoMS@tut.ac.za

Authors

Amos Adeniyi − *Department of Chemical, Metallurgical and Materials Engineering, Tshwane University of Technology, Pretoria 0001, South Africa*

B. Bruce Sithole − *Council for Scientific and Industrial Research (CSIR), South Africa: University of KwaZulu-Natal, Durban 4125, South Africa*

Complete contact information is available at: https://pubs.acs.org/10.1021/acsomega.0c01924

Notes

The authors declare no competing financial interest.

ACKNOWLEDGMENTS

The authors would like to acknowledge the National Research Foundation (NRF) and Department of Science and Technology-Republic of South Africa (DST) for financial support under the "Biorefineries Consortium".

REFERENCES

(1) Deng, S.; Yan, X.; Zhu, Q.; Liao, C. The utilization of reclaimed water: Possible risks arising from waterborne contaminants. *Environ. Pollut.* **2019**, *254*, 113020.

(2) Evans, S.; Campbell, C.; Naidenko, O. V. Cumulative risk analysis of carcinogenic contaminants in United States drinking water. *Heliyon* **2019**, *5*, No. e02314.

(3) Yu, Z.; Hu, C.; Dichiara, A. B.; Jiang, W.; Gu, J. Cellulose Nanofibril/Carbon Nanomaterial Hybrid Aerogels for Adsorption Removal of Cationic and Anionic Organic Dyes. *J. Nanomater.* **2020**, *10*, 169.

(4) Zhang, S.; Li, B.; Wang, X.; Zhao, G.; Hu, B.; Lu, Z.; Wen, T.; Chen, J.; Wang, X. Recent developments of two-dimensional graphene-based composites in visible-light photocatalysis for eliminating persistent organic pollutants from wastewater. *Chem. Eng. J.* **2020**, *390*, 124642.

(5) Ali, I. New Generation Adsorbents for Water Treatment. *Chem. Rev.* **2012**, *112*, 5073−5091.

(6) Wang, Y.; Zhu, L.; Wang, X.; Zheng, W.; Hao, C.; Jiang, C.; Wu, J. Synthesis of aminated calcium lignosulfonate and its adsorption properties for azo dyes. *J. Ind. Eng. Chem.* **2018**, *61*, 321−330.

https://dx.doi.org/10.1021/acsomega.0c01924
ACS Omega 2020, 5, 18798−18807

(7) Ashraf, M. W. Removal of methylene blue dye from wastewater by using supported liquid memberane technology. *Pol. J. Chem. Technol.* **2016**, *18*, 26−30.
(8) Rajabi, M.; Mahanpoor, K.; Moradi, O. Removal of dye molecules from aqueous solution by carbon nanotubes and carbon nanotube functional groups: critical review. *R. Soc. Chem.* **2017**, *18*, 47083.
(9) Basaleh, A. A.; Al-Malack, M. H.; Saleh, T. A. Methylene Blue removal using polyamide-vermiculite nanocomposites: Kinetics, equilibrium and thermodynamic study. *J. Environ. Chem. Eng.* **2019**, *7*, 103107.
(10) Wang, Y.; Bi, N.; Zhang, H.; Tian, W.; Zhang, T.; Wu, P.; Jiang, W. Visible-light-driven photocatalysis-assisted adsorption of azo dyes using Ag2O. *Colloids Surf., A* **2020**, *585*, 124105.
(11) Shavisi, Y.; Sharifnia, S.; Mohamadi, Z. Solar-light-harvesting degradation of aqueous ammonia by CuO/ZnO immobilized on pottery plate: Linear kinetic modeling for adsorption and photocatalysis process. *J. Environ. Chem. Eng.* **2016**, *4*, 2736−2744.
(12) Khan, A.; Wang, J.; Li, J.; Wang, X.; Chen, Z.; Alsaedi, A.; Hayat, T.; Chen, Y.; Wang, X. The role of graphene oxide and graphene oxide-based nanomaterials in the removal of pharmaceuticals from aqueous media: a review. *Environ. Sci. pollut. R* **2017**, *24*, 7938−7958.
(13) Jiang, C.; Wang, X.; Wang, G.; Hao, C.; Li, X.; Li, T. Adsorption performance of a polysaccharide composite hydrogel based on crosslinked glucan/chitosan for heavy metal ions. *Compos. B. Eng.* **2019**, *169*, 45−54.
(14) Pang, X.; Sellaoui, L.; Franco, D.; Dotto, G. L.; Georgin, J.; Bajahzar, A.; Belmabrouk, H.; Lamine, A. B.; Bonilla-Petriciolet, A.; Li, Z. Adsorption of crystal violet on biomasses from pecan nutshell, para chestnut husk, araucaria bark and palm cactus: Experimental study and theoretical modeling via monolayer and double layer statistical physics models. *Chem. Eng. J.* **2019**, *378*, 122101.
(15) Wang, X.; Jiang, C.; Hou, B.; Wang, Y.; Hao, C.; Wu, J. Carbon composite lignin-based adsorbents for the adsorption of dyes. *Chemosphere* **2018**, *206*, 587−596.
(16) Charis, G.; Danha, G.; Muzenda, E. A review of timber waste utilization: Challenges and opportunities in Zimbabwe. *Procedia Manuf.* **2019**, *35*, 419−429.
(17) Li, J.; Xiao, F.; Zhang, L.; Amirkhanian, S. N. Life cycle assessment and life cycle cost analysis of recycled solid waste materials in highway pavement: A review. *J. Cleaner Prod.* **2019**, *233*, 1182−1206.
(18) Lu, H. R.; Qu, X.; El Hanandeh, A. Towards a better environment - the municipal organic waste management in Brisbane: Environmental life cycle and cost perspective. *J. Cleaner Prod.* **2020**, *258*, 120756.
(19) Oyewo, O. A.; Mutesse, B.; Leswifi, T. Y.; Onyango, M. S. Highly efficient removal of nickel and cadmium from water using sawdust-derived cellulose nanocrystals. *J. Environ. Chem. Eng.* **2019**, *7*, 103251.
(20) Nkalane, A.; Oyewo, O. A.; Leswifi, T.; Onyango, M. S. Application of coagulant obtained through charge reversal of sawdust-derived cellulose nanocrystals in the enhancement of water turbidity removal. *Mater. Res.* **2019**, *6*, 105060.
(21) Zhu, X.-l.; Xu, C.-y.; Tang, J.; Hua, Y.-x.; Zhang, Q.-b.; Liu, H.; Wang, X.; Huang, M.-t. Selective recovery of zinc from zinc oxide dust using choline chloride based deep eutectic solvents. *Tran. Nonferrous Met. Soc. China* **2019**, *29*, 2222.
(22) Khoshhesab, Z. M.; Gonbandi, K.; Behbehani, G. R. Removal of reactive black 8 dye from aqueous solution zinc oxide nanoparticles: investigation of adsorption parameters. *Desalin. water treat.* **2014**, *56*, 1558−1565.
(23) Vergheese, T. M.; Sessal, S. S. Environmentally Benign Solar degradation of Methylene Blue dye using Green synthesized ZnO Nanoparticle. *IJGHC.* **2018**, *7*, 265−279.
(24) Hai, L.; Choi, E. S.; Zhai, L.; Panicker, P. S.; Kim, J. Green nanocomposite made with chitin and bamboo nanofibers and its mechanical, thermal and biodegradable properties for food packaging. *Int. J. Biol. Macromol.* **2020**, *144*, 491−499.
(25) Wahid, F.; Duan, Y.-X.; Hu, X.-H.; Chu, L.-Q.; Jia, S.-R.; Cui, J.-D.; Zhong, C. A facile construction of bacterial cellulose/ZnO nanocomposite films and their photocatalytic and antibacterial properties. *Int. J. Biol. Macromol.* **2019**, *132*, 692−700.
(26) Jia, M.; Zhang, X.; Weng, J.; Zhang, J.; Zhang, M. Protective coating of paper works: ZnO/cellulose nanocrystal composites and analytical characterization. *J. Cult. Heritage* **2019**, *38*, 64−74.
(27) Alavi, M.; Nokhodchi, A. An overview on antimicrobial and wound healing properties of ZnO nanobiofilms, hydrogels, and bionanocomposites based on cellulose, chitosan, and alginate polymers. *Carbohydr. Polym.* **2020**, *227*, 115349.
(28) Xiao, H.; Shan, Y.; Zhang, W.; Huang, L.; Chen, L.; Ni, Y.; Boury, B.; Wu, H. C-nanocoated ZnO by TEMPO-oxidized cellulose templating for improved photocatalytic performance. *Carbohydr. Polym.* **2020**, *235*, 115958.
(29) Guan, Y.; Yu, H.-Y.; Abdalkarim, S. Y. H.; Wang, C.; Tang, F.; Marek, J.; Chen, W.-L.; Militky, J.; Yao, J.-M. Green one-step synthesis of ZnO/cellulose nanocrystal hybrids with modulated morphologies and superfast absorption of cationic dyes. *Int. J. Biol. Macromol.* **2019**, *132*, 51−62.
(30) Gibril, M.; Tesfaye, T.; Sithole, B.; Lekha, P.; Ramjugernath, D. Optimisation and enhancement of crystalline nanocellulose production by ultrasonic pretreatment of dissolving wood pulp fibres. *Cellul. Chem. Technol.* **2018**, 52.
(31) Meißner, T.; Oelschlägel, K.; Potthoff, A. Implications of the stability behavior of zinc oxide nanoparticles for toxicological studies. *Int. Nano Lett.* **2014**, *4*, 116.
(32) Ali, A.; Ambreen, S.; Maqbool, Q.; Naz, S.; Shams, M. F.; Ahmad, M.; Phull, A. R.; Zia, M. Zinc impregnated cellulose nanocomposites: Synthesis, characterization and applications. *J. Phys. Chem. Solids* **2016**, *98*, 174−182.
(33) Keshk, S. M. A. S.; Hamdy, M. S. Preparation and physicochemical characterization of zinc oxide/sodium cellulose composite for food packaging. *Turk. J. Chem.* **2019**, *43*, 94−105.
(34) Mashhadzadeh, A. H.; Fathalian, M.; Ahangari, M. G.; Shahavi, M. H. DFT study of Ni, Cu, Cd and Ag heavy metal atom adsorption onto the surface of the zinc-oxide nanotube and zinc-oxide graphene-like structure. *Mater. Chem. Phys.* **2018**, *220*, 366−373.
(35) Mohan, A. C.; Renjanadevi, B. Preparation of Zinc Oxide Nanoparticles and its Characterization Using Scanning Electron Microscopy (SEM) and X-Ray Diffraction(XRD). *Proc. Technol.* **2016**, *24*, 761−766.
(36) Aruchamy, K.; Mahto, A.; Nataraj, S. K. Electrospun nanofibers, nanocomposites and characterization of art: Insight on establishing fibers as product. *Nano-Structures & Nano-Objects.* **2018**, *16*, 45−58.
(37) Díez-Pascual, A. M. 6 - Biodegradable food packaging nanocomposites based on ZnO-reinforced polyhydroxyalkanoates. In *Food Packaging*; Grumezescu, A. M., editor.Academic Press, 2017, 185−221.
(38) Fadillah, G.; Saleh, T. A.; Wahyuningsih, S.; Putri, E. N. K.; Febrianastuti, S. Electrochemical removal of methylene blue using alginate-modified graphene adsorbents. *Chem. Eng. J.* **2019**, *378*, 122140.
(39) Popescu, C.-M.; Jones, D.; Schalnat, J.; Segerholm, K.; Henriksson, M.; Westin, M. Structural characterization and mechanical properties of wet-processed fibreboard based on chemo-thermomechanical pulp, furanic resin and cellulose nanocrystals. *Int. J. Biol. Macromol.* **2019**, *145*, 586−593.
(40) Moghaddas, S. M. T. H.; Elahi, B.; Javanbakht, V. Biosynthesis of pure zinc oxide nanoparticles using Quince seed mucilage for photocatalytic dye degradation. *J. Alloys Compd.* **2020**, *821*, 153519.
(41) Shah, A. A.; Bhatti, M. A.; Tahira, A.; Chandio, A. D.; Channa, I. A.; Sahito, A. G.; Ebrahim, C.; Willander, W.; Nur, O.; Ibupoto, Z. H. Facile synthesis of copper doped ZnO nanorods for the efficient photo degradation of methylene blue and methyl orange. *Ceram. Int.* **2020**, *46*, 9997−10005.

https://dx.doi.org/10.1021/acsomega.0c01924
ACS Omega 2020, 5, 18798−18807

(42) Brar, S. K.; Wangoo, N.; Sharma, R. K. Enhanced and selective adsorption of cationic dyes using novel biocompatible self-assembled peptide fibrils. *J. Environ. Manage.* **2020**, *255*, 109804.
(43) Mantasha, I.; Hussain, S.; Ahmad, M.; Shahid, M. Two dimensional (2D) molecular frameworks for rapid and selective adsorption of hazardous aromatic dyes from aqueous phase. *Sep. Purif. Technol.* **2020**, 116413.
(44) Fan, L.; Zhang, Y.; Luo, C.; Lu, F.; Qiu, H.; Sun, M. Synthesis and characterization of magnetic β-cyclodextrin−chitosan nanoparticles as nano-adsorbents for removal of methyl blue. *Int. J. Biol. Macromol.* **2012**, *50*, 444−450.
(45) Jabli, M.; Almalki, S. G.; Agougui, H. An insight into methylene blue adsorption characteristics onto functionalized alginate biopolymer gel beads with λ-carrageenan-calcium phosphate,carboxymethyl cellulose, and celite 545. *Int. J. Biol. Macromol.* **2020**, 1091.
(46) Sakr, F.; Alahiane, S.; Sennaoui, A.; Dinne, M.; Bakas, I.; Assabbane, A. Removal of cationic dye (Methylene Blue) from aqueous solution by adsorption on two type of biomaterial of South Morocco. *Mater. Today Proceed.* **2020**, *22*, 93−96.
(47) Amode, J. O.; Santos, J. H.; Alam, Z.; Mirza, A. H.; Mei, C. C. Adsorption of methylene blue from aqueous solution using untreated and treated (Metroxylon spp.) waste adsorbent: equilibrium and kinetics studies. *Internet J. Chem.* **2016**, *7*, 333.
(48) Maguana, Y. E.; Elhadiri, N.; Bouchdoug, M.; Benchanaa, M.; Boussetta, A. Optimization of Preparation Conditions of Novel Adsorbent from Sugar Scum Using Response Surface Methodology for Removal of Methylene Blue. *J. Chem.* **2018**, 2093654.
(49) Rupa, M. J.; Pal, A.; Saha, B. B. Activated carbon-graphene nanoplatelets based green cooling system: Adsorption kinetics, heat of adsorption, and thermodynamic performance. *Energy* **2020**, *193*, 116774.
(50) Hubbe, M. A.; Azizian, S.; Douven, S. Implications of apparent pseudo-second-order adsorption kinetics onto cellulosic materials: A review. *BioResources* **2019**, *14*, 7582−7626.
(51) Mohamed, A. K.; Mahmoud, M. E. Metoprolol beta-blocker decontamination from water by the adsorptive action of metal-organic frameworks-nano titanium oxide coated tin dioxide nanoparticles. *J. Mol. Liq.* **2020**, *309*, 113096.
(52) Batool, F.; Akbar, J.; Iqbal, S.; Noreen, S.; Bukhari, S. N. A. Study of Isothermal, Kinetic, and Thermodynamic Parameters for Adsorption of Cadmium: An Overview of Linear and Nonlinear Approach and Error Analysis. *Bioinorg. Chem. Appl.* **2018**, *2018*, 3463724.
(53) Mahmoud, M. E.; Amira, M. F.; Seleim, S. M.; Mohamed, A. K. Amino-decorated magnetic metal-organic framework as a potential novel platform for selective removal of chromium (Vl), cadmium (II) and lead (II). *J. Hazard. Mater.* **2020**, *381*, 120979.
(54) Zhou, L.; Huang, J.; He, B.; Zhang, F.; Li, H. Peach gum for efficient removal of methylene blue and methyl violet dyes from aqueous solution. *Carbohydr. Polym.* **2014**, *101*, 574−581.
(55) Li, Q.; Yue, Q.-Y.; Su, Y.; Gao, B.-Y.; Li, J. Two-step kinetic study on the adsorption and desorption of reactive dyes at cationic polymer/bentonite. *J. Hazard. Mater.* **2009**, *165*, 1170−1178.

https://dx.doi.org/10.1021/acsomega.0c01924
ACS Omega 2020, 5, 18798−18807